ORGANOMETALLICS

pubs.acs.org/Organometallics

Article

Ortho-Fluoro Effect on the C−C Bond Activation of Benzonitrile Using Zerovalent Nickel

Sébastien Lachaize,[§] Dominique C. Gallegos,[§] Juliana J. Antonio, Abdurrahman C. Atesin,* Tülay A. Ateşin,* and William D. Jones*

Cite This: *Organometallics* 2023, 42, 2134−2147

Read Online

ACCESS | Metrics & More | Article Recommendations | Supporting Information

ABSTRACT: The effect of fluoro substitution on the C−C bond activation of aromatic nitriles has been studied by reacting a variety of fluorinated benzonitriles with the nickel(0) fragment [Ni(dippe)] and by locating the reaction intermediates and transition-state structures on the potential energy surface by using density functional theory calculations with the [Ni(dmpe)] fragment (dippe = 1,2-bis(diisopropylphosphino)ethane, dmpe = 1,2-bis(dimethylphosphino)ethane). As in the previous reports, the reaction of fluorinated benzonitriles with the [Ni(dippe)] fragment initially formed an η^2-nitrile complex, which then converted to the C−CN bond activation product. Thermodynamic parameters for the equilibrium between these complexes have been determined experimentally in both a polar (tetrahydrofuran) and a nonpolar (toluene) solvent for 3-fluoro- and 4-fluorobenzonitrile. The stability of the C−C bond activation products is shown to be strongly dependent on the number of *ortho*-F substituents (−6.6 kcal/mol per *o*-F) and only slightly dependent on the number of *meta*-F substituents (−1.8 kcal/mol per *m*-F).

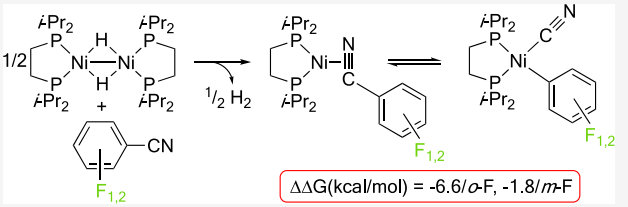

INTRODUCTION

Carbon−carbon (C−C) bond activation and functionalization have gained increasing attention as an alternative synthetic method to the more conventional methods in complex molecule synthesis. Despite its abundance, there are only a few methods known for the C−C bond activation and more general methods are needed.[1−6] The activation of C−C bonds with homogeneous transition-metal complexes under mild conditions is a great challenge due to the kinetic inaccessibility and thermodynamic stability of C−C single bonds. In early examples, the relief of ring strain has been used as an effective strategy for C−C bond activation.[7] Besides strain assistance, aromatization[8] and proximity effect using a directing group[9,10] are several other strategies used to activate C−C bonds in unstrained molecules. The C−C bonds next to carbonyl or cyano groups in unstrained molecules can be activated without the assistance of a directing group.[11−16] The activation of C−C bonds in strained molecules has been more developed than that in unstrained molecules.[17−22]

The increasing cost of noble metals has led to the resurgence of interest in the use of earth-abundant metals. Our group and others used the direct oxidative addition of low-valent nickel complexes into the C−CN bonds of aliphatic,[23−26] aromatic,[27−39] and allylic[40−53] nitriles.[54−61] Scheme 1 shows the C−CN bond activation of benzonitrile using the hydride-bridged nickel dimer, $[Ni(dippe)(\mu\text{-}H)]_2$ (dippe = 1,2-bis(diisopropylphosphino)ethane).[31] This dimer releases H_2 gas to generate the [Ni(dippe)] fragment, which reacts with benzonitrile to give η^2-nitrile and η^2-arene complexes at low temperatures. At room temperature, η^2-arene complexes were converted to η^2-nitrile complexes, which then equilibrated with the C−CN bond activation product [(dippe)Ni(Ph)(CN)]. Thermodynamic parameters for the equilibrium have been obtained in both tetrahydrofuran (THF) and toluene. η^2-Arene intermediates and the transition state (TS) structures on the potential energy surface (PES) between the η^2-nitrile complex and the C−CN bond activation product were located by density functional theory (DFT) calculations. The fluxionality of the η^2-arene complex was demonstrated both experimentally and computationally. In the reactions of polycyclic aromatic

Scheme 1. Reaction of $[Ni(dippe)(\mu\text{-}H)]_2$ with Benzonitrile

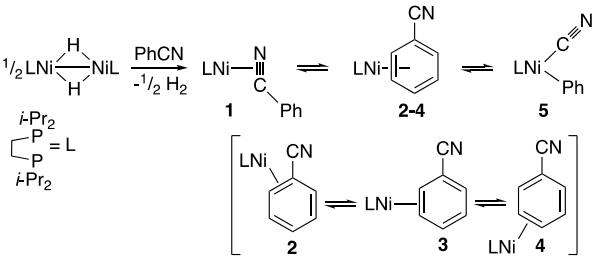

Received: June 16, 2023
Published: July 21, 2023

nitriles, the η^2-arene complex can exist as a stable species.[32] The C−CN bond activation of benzonitrile followed by subsequent transformation has been utilized to synthesize natural alkaloids via asymmetric intramolecular arylcyanation of alkenes, demonstrating the power of this reaction in complex molecule synthesis.[62,63]

Benzonitriles are found in many natural products[64] and pharmaceuticals,[65] and the nitrile group can be easily converted into other functional groups.[66] In this study, we incorporated the fluoro-functionality due to the increasing interest in fluoro-pharmaceuticals.[67] The unique properties of fluorine (the second smallest atom, most electronegative element) often lead to enhanced pharmacokinetic and physicochemical properties such as improved metabolic stability and enhanced membrane permeation. In this report, we investigate the effect of fluoro substitution on the C−CN bond activation of 2-fluoro-, 3-fluoro-, 4-fluoro-, 2,6-difluoro-, and 3,5-difluorobenzonitrile with the [Ni(dippe)] fragment in tetrahydrofuran and toluene (Scheme 2). Reaction pathways

Scheme 2. Reaction of [Ni(dippe)(μ-H)]$_2$ with Fluorinated Benzonitriles

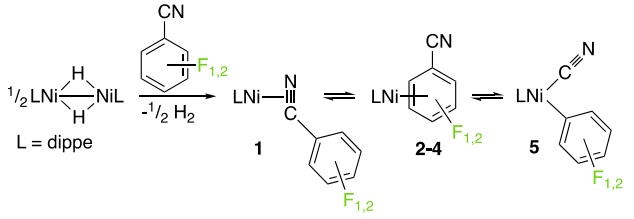

leading to the formation of the C−CN bond activation products and the energies of the intermediates and the TS structures along the way were examined using DFT calculations with the [Ni(dmpe)] fragment (dmpe = 1,2-bis(dimethylphosphino)ethane). The insight gained from this mechanistic study can be used to develop new strategies for C−C bond activation and incorporating fluorine in the products.

RESULTS AND DISCUSSION

C−CN Bond Activation of 2-Fluorobenzonitrile. The reaction of 2-fluorobenzonitrile with [Ni(dippe)(μ-H)]$_2$ gave (dippe)Ni(η^2-2-F-C$_6$H$_4$CN), **1a**, which showed a pair of doublets in the ^{31}P{^{1}H} NMR spectrum (THF-d_8) at δ 66.6 and 77.8 (J_{P-P} = 68 Hz). When the solution was heated at 74 °C for 1 day, (dippe)Ni(2-F-C$_6$H$_4$)(CN), **5a**, formed. The ^{31}P{^{1}H} NMR spectrum (tol-d_8) of **5a** showed a doublet at δ 75.5 (J_{P-P} = 27 Hz) and a doublet of doublets at δ 84.7 (J_{P-P} = 27, J_{P-F} = 10 Hz). All X-ray single-crystal structures are shown in Figure 1.

C−CN Bond Activation of 3-Fluorobenzonitrile. The reaction of 3-fluorobenzonitrile with [Ni(dippe)(μ-H)]$_2$ gave (dippe)Ni(η^2-3-F-C$_6$H$_4$CN), **1b**, which showed a pair of doublets in the ^{31}P{^{1}H} NMR spectrum (THF-d_8) at δ 67.7 and 79.3 (J_{P-P} = 65 Hz). When the solution was heated at 43.7 °C for 5 days, NMR spectra showed mostly (~95%) (dippe)Ni(3-F-C$_6$H$_4$)(CN), **5b**. The ^{31}P{^{1}H} NMR spectrum (THF-d_8) of **5b** showed a pair of doublets at δ 73.3 and 83.9 (J_{P-P} = 22 Hz).

C−CN Bond Activation of 4-Fluorobenzonitrile. The reaction of 4-fluorobenzonitrile with [Ni(dippe)(μ-H)]$_2$ gave (dippe)Ni(η^2-4-F-C$_6$H$_4$CN), **1c**, which showed a pair of doublets in the ^{31}P{^{1}H} NMR spectrum (THF-d_8) at δ 68.0 and 80.0 (J_{P-P} = 66 Hz). When the solution was heated at 70 °C for several days, NMR spectra showed mostly (~85%) (dippe)Ni(4-F-C$_6$H$_4$)(CN), **5c**. The ^{31}P{^{1}H} NMR spectrum (THF-d_8) of **5c** showed a pair of doublets at δ 72.0 and 82.5 (J_{P-P} = 22 Hz).

C−CN Bond Activation of 2,6-Difluorobenzonitrile. The reaction of 2,6-difluorobenzonitrile with [Ni(dippe)(μ-H)]$_2$ gave (dippe)Ni(η^2-2,6-F$_2$-C$_6$H$_3$CN), **1d**, which showed a pair of doublets in the ^{31}P{^{1}H} NMR spectrum (THF-d_8) at δ 68.4 and 78.8 (J_{P-P} = 67 Hz). When the solution was heated at 70 °C for 1 month, (dippe)Ni(2,6-F$_2$-C$_6$H$_3$)(CN), **5d**, formed completely. The ^{31}P{^{1}H} NMR spectrum (THF-d_8) of **5d** showed a doublet at δ 79.5 (J_{P-P} = 32 Hz) and a doublet of triplets at δ 87.5 (J_{P-P} = 32, J_{P-F} = 9 Hz).

C−CN Bond Activation of 3,5-Difluorobenzonitrile. The reaction of 3,5-difluorobenzonitrile with [Ni(dippe)(μ-H)]$_2$ gave (dippe)Ni(η^2-3,5-F$_2$-C$_6$H$_3$CN), **1e**, which showed a pair of doublets in the ^{31}P{^{1}H} NMR spectrum (THF-d_8) at δ 68.3 and 80.1 (J_{P-P} = 62 Hz). When the solution was heated at 70 °C overnight, NMR spectra showed the formation of (dippe)Ni(3,5-F$_2$-C$_6$H$_3$)(CN), **5e**, in ~68% yield. The ^{31}P{^{1}H} NMR spectrum (THF-d_8) of **5e** showed a pair of doublets at δ 74.3 and 85.4 (J_{P-P} = 23 Hz).

Comparison of the X-ray Single-Crystal Structure of the η^2-Nitrile Complexes. Table 1 summarizes the interatomic distances (Å) around the nickel metal center in

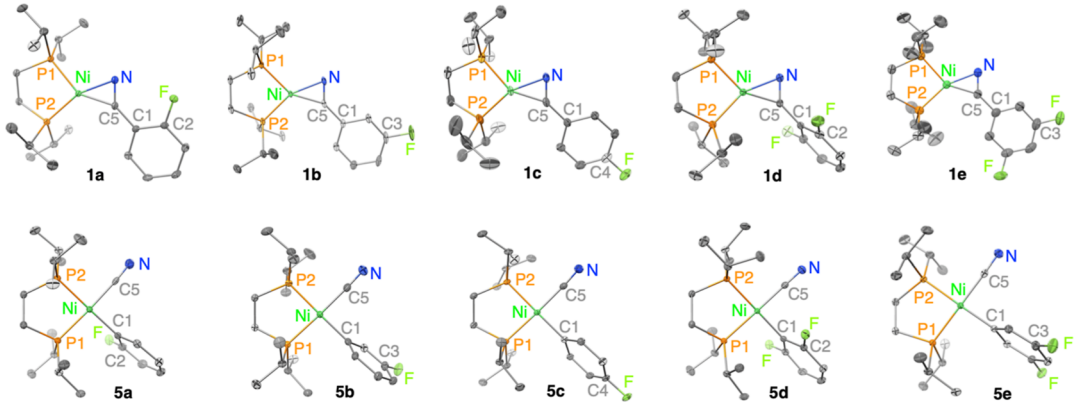

Figure 1. ORTEP drawings of η^2-CN complexes **1a−e** and C−CN bond activation products, **5a−e**. Displacement ellipsoids are shown at the 50% probability level. Hydrogen atoms are omitted for clarity.

https://doi.org/10.1021/acs.organomet.3c00275
Organometallics 2023, 42, 2134−2147

Table 1. Interatomic Distances (Å) around the Ni Metal Center in the X-ray Single-Crystal Structures of 1a−1e

	Ni−C5	Ni−N	Ni−P1	Ni−P2
1a	1.8642(13)	1.9088(12)	2.1524(4)	2.1771(4)
1b	1.8523(19)	1.9181(17)	2.1480(7)	2.1783(7)
1c	1.8519(14)	1.9093(13)	2.1446(4)	2.1670(5)
1d	1.8430(11)	1.9268(10)	2.1348(3)	2.1730(3)
1e	1.8488(14)	1.9038(13)	2.1445(4)	2.1779(4)
Ph[29]	1.867(4)	1.908(3)	2.1464(12)	2.1729(12)

the X-ray single-crystal structure of the η^2-nitrile complexes (**1a−e**). The coordination environment of the nickel metal center is square planar with two phosphorus atoms from the dippe ligand, and the carbon and nitrogen atoms of the nitrile group occupying the four coordination sites. The interatomic distance between C5 and N [1.2243(19)−1.233(2) Å] is elongated compared to free benzonitrile (1.136 Å), indicating a decrease in bond order. The nitrile group deviates from linearity with the C1−C5−N angle (α) of 135.01(10)−140.19(11)°, consistent with the sp^2 hybridization of the nitrile carbon atom instead of sp hybridization. Similar to the previously reported η^2-nitrile complex of benzonitrile,[29] the P1−Ni−P2 plane is almost coplanar with the C5−Ni−N plane (β), with a slight deviation of 1.73−4.82° twist angle. The angle between the P1−Ni−P2 plane and the plane of the phenyl group (γ) varies more with a twist angle of 2.81° in **1e**, 9.49−13.36° in **1a-c**, and 86.41° in **1d** compared to 10.63° in benzonitrile. The perpendicularity of the phenyl group in **1d** can be attributed to an additional steric interaction between the two *ortho*-fluoro substituents and the dippe ligand (see Figure SI30 for a comparison of C2−C1−C5−N dihedral angle scan in the η^2-nitrile complexes of 2,6-difluorobenzonitrile with [Ni(dmpe)] and [Ni(dippe)] fragments).

Comparison of the X-ray Single-Crystal Structure of the C−CN Bond Activation Products. Table 2 summarizes

Table 2. Interatomic Distances (Å) around the Ni Metal Center in the X-Ray Single-Crystal Structures of 5a−5e

	Ni−C1	Ni−C5	Ni−P1	Ni−P2
5a	1.9340(13)	1.9095(13)	2.1892(6)	2.1783(5)
5b	1.9305(9)	1.8805(9)	2.1926(3)	2.1781(2)
5c	1.9370(12)	1.8814(13)	2.1919(4)	2.1771(4)
5d	1.9326(10)	1.8783(10)	2.1962(3)	2.1887(3)
5e	1.9279(9)	1.8784(9)	2.1929(3)	2.1792(2)
Ph[29]	1.935(2)	1.877(3)	2.1959(7)	2.1773(7)

the interatomic distances (Å) around the nickel metal center in the X-ray single-crystal structure of the C−CN bond activation products (**5a−5e**). These structures also show a square planar molecular geometry around the nickel metal center similar to the previously reported C−CN bond activation product of benzonitrile.[29] The interatomic distance between C5 and N (1.1059(17)-1.1551(14) Å) is closer to a bond order of 3, with varying degrees of π-back donation from the nickel metal center to the cyano ligand. The Ni−P2 bonds *trans* to the cyano ligand are elongated [2.1771(4)−2.1887(3) Å] compared to the Ni−P1 bonds *trans* to the N atom in the η^2-nitrile complexes [2.1348(3)−2.1524(4) Å]. This is consistent with the greater *trans* influence of the cyano ligand. The closest distance between the C−H of the dippe ligand and the centroid of the phenyl ring is 2.594−2.796 Å, and the closest distances between the ligand and the fluoro substituents are 2.475 Å in **5a** and 2.435 and 2.447 Å in **5d**. In all cases, the phenyl ring is almost perpendicular to the P1−Ni−P2 plane, with a twist angle (γ) of 69.31−76.58°.

Thermodynamics of the C−CN Bond Activation. The equilibrium ratios of the η^2-nitrile complex, **1b**, and the C−CN bond activation product, **5b**, formed from the reaction of $[Ni(dippe)(\mu\text{-}H)]_2$ with 3-fluorobenzonitrile were measured in THF-d_8 and toluene-d_8 at various temperatures. Similarly, the equilibrium ratios of the η^2-nitrile complex, **1c**, and the C−CN bond activation product, **5c**, formed from the reaction with 4-fluorobenzonitrile were measured in THF-d_8 and toluene-d_8 at various temperatures. The Van't Hoff plots are shown in Figure 2.

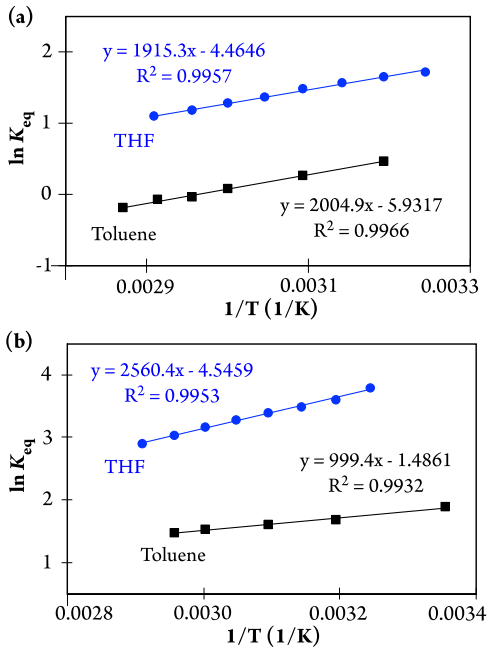

Figure 2. Van't Hoff plot for the equilibrium in THF and toluene over the range of 25−75 °C between (a) **1b** and **5b** and (b) **1c** and **5c** in the reaction of $[Ni(dippe)(\mu\text{-}H)]_2$ with 3-fluorobenzonitrile and 4-fluorobenzonitrile, respectively.

The thermodynamic parameters were determined from the Van't Hoff plots and are shown in Table 3 for both THF and

Table 3. Thermodynamic Parameters Determined from the Van't Hoff Plots

	$\Delta H°$ (kcal/mol)	$\Delta S°$ (e.u.)	$\Delta G°$ (kcal/mol)
3F(THF)	−5.09 ± 0.14	−9.0 ± 0.4	−2.39(4)
3F(Tol)	−1.99 ± 0.09	−3.0 ± 0.3	−1.10(5)
4F(THF)	−3.81 ± 0.10	−8.9 ± 0.3	−1.16(1)
4F(Tol)	−3.98 ± 0.12	−11.8 ± 0.4	−0.47(0)
H(THF)[29]	−3.52 ± 0.07	−9.3 ± 0.2	−0.74(2)
H(Tol)[29]	−4.09 ± 0.22	−13.4 ± 0.7	−0.07(6)

toluene. Equilibrium constants for the other fluorobenzonitrile substrates (**1a**/**5a**, **1d**/**5d**, and **1e**/**5e**) could not be calculated since there were not enough η^2-nitrile complexes (**1a**, **1d**, and **1e**) left in solution to measure its concentration reliably by NMR spectroscopy.

https://doi.org/10.1021/acs.organomet.3c00275
Organometallics 2023, 42, 2134−2147

The free energies ($\Delta G°$) for C−CN oxidative addition for both 3-fluoro and 4-fluorobenzonitrile in THF and toluene are negative at room temperature, indicating that the formation of the C−CN bond activation products from the η^2-nitrile complexes is energetically downhill. The electronegative fluoro substituent drives the equilibrium further toward the products. Similar to benzonitrile, the Gibbs free energy of the reaction is more negative in THF compared to toluene.[31] The more polar solvent, THF, stabilizes the C−CN bond activation products more in comparison to the η^2-nitrile complexes, shifting the equilibrium further toward the products.

DFT Calculations. Reaction intermediates and TS structures between the η^2-nitrile, η^2-arene, and the C−CN bond activation products during the reaction of fluorinated benzonitriles were located in the gas phase using DFT calculations. The [Ni(dippe)] fragment used in the experiments was replaced with the [Ni(dmpe)] fragment. Only the η^2-nitrile complex, **1**, and the C−CN bond activation product, **5**, are stable enough to be isolated and characterized experimentally and X-ray single-crystal structures of **1** and **5** were used as a starting structure for the geometry optimizations. For comparison purposes, the reaction of benzonitrile was revisited (Scheme 3) and included in the analysis of fluorinated benzonitrile reactions. All the optimized structures on the PES of the C−CN bond activation of benzonitrile (Figure SI6), selected bond lengths (Table SI7), and angles (Table SI13) are summarized in the Supporting Information and will be discussed in comparison to other fluorinated benzonitriles later in the text.

Scheme 3. Reaction Intermediates and TS Structures on PES of C−CN Bond Activation of Benzonitrile with [Ni(dmpe)]

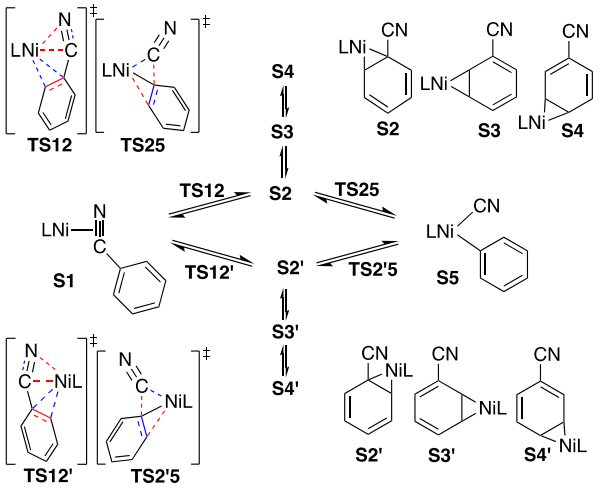

The potential energy surface between the η^2-nitrile complex, **S1**, and the C−CN bond activation product, **S5**, is mapped by varying the C−CN interatomic distance and the dihedral angle between the phenyl ring and the P−Ni−P plane (γ). Solvation-corrected Gibbs free energies were calculated by using the gas phase-optimized structures and solvent density model (SMD) in THF and toluene. Using the thermodynamic parameters for the equilibrium in both polar and nonpolar solvents, we added appropriate corrections to the calculated energies. Structures **S1** and **S5** are connected through two sets of two TS structures, **TS12**/**TS12′** and **TS25**/**TS2′5**, and the corresponding η^2-arene intermediates, **S2**/**S2′** (Figure SI17). In **S2**, the nickel metal center is coordinated to the phenyl ring through the **C1** and **C2** carbon atoms, whereas it is coordinated through the **C1** and **C2′** carbon atoms in **S2′**. These two geometries are distinct due to the puckering of the Ni(dmpe) ring, which places one of the methyl groups on each phosphorus closer to the nitrile. Structures **S2**/**S2′**, **S3**/**S3′**, and **S4**/**S4′** are the two sets of three possible η^2-arene intermediates, in which nickel metal is coordinated on opposite sides of the phenyl ring. Six transition-state structures, **TS22′**, **TS23**/**TS2′3′**, **TS34**/**TS3′4′**, and **TS44′**, were located for the migration of the nickel metal between these intermediates (Figure SI18). These can be described as η^2 to η^3 to η^2 pathways. In the following sections, η^2-nitrile and η^2-arene intermediates and C−CN bond activation products are each discussed in detail.

Optimized Structures of the η^2-Nitrile Complexes. There are two possible structures for the η^2-nitrile complexes with 2-fluorobenzonitrile, **Sa1** and **Sa′1**, resulting from the position of the fluoro substituent with respect to the nickel metal center. Gas phase-optimized structures of **Sa1** and **Sa′1** are shown in Figure 3. **Sa1** has the fluoro substituent on the **C2** carbon atom, which is on the same side as the nickel metal center, whereas **Sa′1** has the fluoro substituent away from the nickel metal center at the **C2′** carbon atom. The Gibbs free energy of **Sa1** relative to **Sa′1** is +1.3 kcal/mol in THF and +0.5 kcal/mol in toluene and the lowest energy barrier for the phenyl rotation, **TSaa′1**, is 2.3 kcal/mol in THF and 2.1 kcal/mol in toluene. Due to the negligible rotational barrier of the phenyl ring and low energy difference between **Sa1** and **Sa′1**, both structures exist in solution.

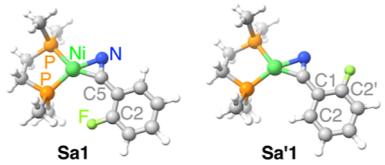

Figure 3. Gas phase-optimized structures of **Sa1** and **Sa′1**.

The optimized structures of **Sa1** and **Sa′1** are in good agreement with the experimental structure of **1a** with the dippe ligand discussed earlier. The nitrile group deviates from linearity with a C1−C5−N angle (α) of 135.4° in **Sa1** and 139.0° in **Sa′1**, which is consistent with 137.10(13)° in the X-ray single-crystal structure of **1a**. The coordination environment around the nickel metal center is square planar with small twist angles of 1.37° (**Sa1**) and 1.11° (**Sa′1**) between P1−Ni−P2 and C5−Ni−N planes (β) compared to 2.10° in the X-ray single-crystal structure of **1a**. The coordinated C5−N bond is slightly longer in **Sa1** (1.238 Å) and **Sa′1** (1.234 Å) compared to 1.2290(17) Å in the X-ray single-crystal structure of **1a**. The phenyl ring is almost coplanar with the P−Ni−P plane (γ) in **Sa′1** with a small twist angle of 1.55°, whereas in **Sa1**, it is considerably deviated from planarity with a twist angle of 9.20° due to steric hindrance (see Supporting Information, Tables SI1 and SI2 for a more comprehensive list of bond lengths and Table SI8 for angles).

Similar to 2-fluorobenzonitrile, there are two possible structures of η^2-nitrile complexes with 3-fluorobenzonitrile, **Sb1** and **Sb′1**, due to the unsymmetric substitution of the phenyl ring with no significant energy difference between them. Similarly, for the other fluorobenzonitriles, gas phase-optimized structures of **Sa1**−**Se1** and **S1** are shown in Figures

https://doi.org/10.1021/acs.organomet.3c00275
Organometallics 2023, 42, 2134−2147

Table 4. Selected Interatomic Distances (Å) and Angles (°) for the Optimized Structures of Sa1−Se1 and S1

	Ni−C5	Ni−N	C5−N	C1−C5	γ^a
Sa1/Sa′1	1.859/1.875	1.899/1.900	1.238/1.234	1.463/1.461	9.20/1.55
Sb1/Sb′1	1.870/1.871	1.902/1.900	1.235/1.235	1.466/1.466	1.19/1.49
Sc1	1.873	1.901	1.235	1.464	0.80
Sd1	1.862	1.896	1.238	1.459	12.78
Se1	1.867	1.901	1.235	1.467	1.06
S1	1.874	1.901	1.234	1.466	1.70

[a]Angle between the P−Ni−P plane and the phenyl ring.

SI1−SI6. Comparisons of selected interatomic distances (Å) and angles (°) for these structures are summarized in Table 4, and a comprehensive list of structural parameters for all optimized structures are summarized in Tables SI1−SI13. The average bond lengths for Ni−C5, Ni−N, C5−N, and C1−C5 are 1.869, 1.900, 1.236, and 1.464 Å, respectively. The deviation from linearity of the nitrile group (α) is 137.25° on average. The C1−C5 bond length is the shortest in **Sd1** (1.459 Å) as in the X-ray single-crystal structure of **1d** (1.4676(16) Å). The C5−N bond length ranges from 1.234 to 1.238 Å with the sterically demanding *ortho* substitution resulting in the longest bond lengths in **Sa1** and **Sd1**. The steric effect of *ortho* substituents is greater on the coplanarity of the P−Ni−P plane and the phenyl ring (γ) with the largest deviation of 12.78° in **Sd1** compared to 9.20° in **Sa1** and 0.80−1.70° for other substrates. As a general trend, the *ortho* substitution on the same side of the nickel metal center leads to shorter Ni−C5, Ni−N, and C1−C5, longer C5−N bond lengths, and a larger deviation from linearity of the nitrile group.

The disparity in the angle between the P−Ni−P plane and the phenyl ring (γ) in the X-ray single-crystal structure of **1d** (86.41°) and the optimized structure of **Sd1** (12.78°) by the DFT calculations is likely a result of the less sterically encumbered [Ni(dmpe)] model. In fact, the structure with almost perpendicular phenyl ring as in **1d** is located as a TS structure with a very low-energy rotational barrier of the phenyl ring of 0.6 kcal/mol in THF and 0.7 kcal/mol in toluene relative to **Sd1**.

Optimized Structures of the η^2-Arene Intermediates. There are two possible structures of three different η^2-arene intermediates, **S2/S2′**, **S3/S3′**, and **S4/S4′**. In the first set (**S2/S2′**), the nickel metal center is coordinated to the phenyl ring through the C═C double bond between the **C1** and **C2/C2′** carbon atoms next to the cyano group. In the second (**S3/S3′**) and third (**S4/S4′**) sets, the nickel metal center is coordinated to the phenyl ring through the C═C double bond between the **C2/C2′**and **C3/C3′** carbon atoms and **C3/C3′**and **C4/C4′** carbon atoms, respectively. Our previous studies revealed that **S2/S2′** is a crucial intermediate leading to C−C bond activation.[31] Below is a discussion on this intermediate. Similarly, **S3/S3′** and **S4/S4′** are discussed in the Supporting Information.

Gas phase-optimized structures of **Sa2** and **Sa2′** are shown in Figure 4. In **Sa2**, the nickel metal center is coordinated to the phenyl ring through the **C1** and **C2** carbon atoms, whereas it is coordinated through the **C1** and **C2′** carbon atoms in **Sa2′**. In both **Sa2** and **Sa2′**, the fluoro substituent is on the **C2** carbon atom. The structures that have the fluoro substituent on the **C2′** carbon atom are labeled as **Sa′2** and **Sa′2′** (see Figure SI1 for the gas phase-optimized structures). The average length of the C═C double bond between the **C1** and **C2/C2′** carbon atoms is 1.468 Å when the nickel metal center is coordinated compared to 1.447 Å when it is not. When the nickel metal center and the fluoro substituent are on the same side (**Sa2** and **Sa′2′**), the Ni−C1 bonds are longer and the Ni−C2/C2′ bonds are shorter than when they are on opposite sides (**Sa′2** and **Sa2′**) due to electronic effects. Both C5−N and C1−C5 bonds are shorter than in the η^2-nitrile complexes (1.434 vs 1.464 Å and 1.168 vs 1.236 Å, respectively). The nitrile group is almost linear with an average angle (α) of 177.75°. The angle between the P−Ni−P plane and the phenyl ring (γ) is much smaller in **Sa2** and **Sa′2′** than in **Sa′2** and **Sa2′** (64.76 and 58.67° vs 72.09 and 77.08°).

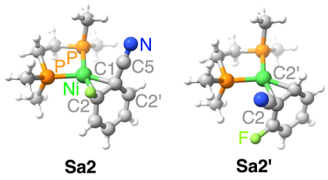

Figure 4. Gas phase-optimized structures of **Sa2** and **Sa2′**.

Selected interatomic distances (Å) and angles (°) for the optimized structures of **Sa2−Se2** and **S2** with their relative Gibbs free energies with respect to corresponding **Sa1−Se1** and **S1** in THF and toluene (in parenthesis) are summarized in Table 5. Structures labeled as **b** have the same designations regarding the position of the nickel metal center and the fluoro

Table 5. Selected Interatomic Distances (Å), Angles (°), and Relative Gibbs Free Energies (kcal/mol) for Sa2−Se2 and S2

	Ni−C1	Ni−C2/2′	γ^a	$\Delta G^{\circ b}$
Sa2	2.005	1.937	64.76	9.9 (9.6)
Sa′2	1.983	1.996	72.09	9.1 (8.4)
Sa2′	1.978	1.999	77.08	9.3 (8.5)
Sa′2′	2.015	1.925	58.67	10.3 (9.9)
Sb2	2.014	1.960	68.57	8.3 (8.0)
Sb′2	1.998	1.993	69.12	10.5 (10.2)
Sb2′	1.999	1.992	69.01	9.2 (9.2)
Sb′2′	2.012	1.964	58.67	8.0 (7.8)
Sc2	2.006	1.985	68.08	10.4 (10.1)
Sc2′	2.008	1.985	66.19	9.4 (9.2)
Sd2	1.984	1.941	67.97	6.9 (7.1)
Sd2′	1.995	1.928	60.64	7.0 (7.2)
Se2	2.003	1.966	67.50	8.1 (7.9)
Se2′	2.004	1.965	70.08	7.6 (7.6)
S2	2.005	1.992	68.82	10.7 (10.2)
S2′	2.007	1.992	66.70	9.5 (9.2)

[a]Angle between the P−Ni−P plane and the phenyl ring. [b]Relative Gibbs free energies calculated with respect to corresponding **S1** in THF (numbers in the parenthesis are in toluene).

https://doi.org/10.1021/acs.organomet.3c00275
Organometallics 2023, 42, 2134−2147

substituent, except that the substituent is on the C3/C3′ carbon atoms instead of C2/C2′ (see Figure SI2 for gas phase-optimized structures for **Sb2** and Figures SI3–SI6 for **Sc2**-**Se2** and **S2**). Average Ni–C1 and Ni–C2/C2′ bond lengths are 2.001 Å and 1.970 Å, respectively. The shortest Ni–C1 bond lengths (1.978 Å in **Sa2′**, 1.983 Å in **Sa′2**, and 1.984 Å in **Sd2**) and Ni–C2/C2′ bond lengths (1.925 Å in **Sa′2′** and 1.928 Å in **Sd2′**) can be attributed to the electronic effects of the fluoro substituents. The average angle between the P–Ni–P plane and the phenyl ring (γ) is 67.12°. The C1–C5, C5–N bond lengths and C1–C5–N angle (α) are relatively constant regardless of the position of the nickel metal center and the fluoro substitution (see Tables SI1–SI13 for a more comprehensive list of structural parameters). The average relative Gibbs free energy of **Sa2**–**Se2**, **S2** with respect to corresponding **Sa1**–**Se1**, **S1** is 9.0 kcal/mol in THF and 8.8 kcal/mol in toluene. **Sd2** and **Sd2′** have the lowest energies.

Optimized Structures of the C–CN Bond Activation Products. There are two possible structures for the C–CN bond activation product of 2-fluorobenzonitrile, **Sa5** and **Sa′5**, as a result of the free rotation around the phenyl ring with a barrier of 4.3 kcal/mol in THF and 5.8 kcal/mol in toluene. Gas phase-optimized structures of **Sa5** and **Sa′5** shown in Figure 5 are in good agreement with the experimental structure

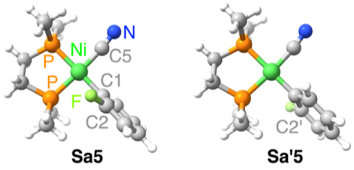

Figure 5. Gas phase-optimized structures of **Sa5** and **Sa′5**.

of **5a** with the dippe ligand discussed earlier. The phenyl ring is almost perpendicular to the square plane of the complex with twist angles of 80.84° (**Sa5**) and 77.58° (**Sa′5**) between P1–Ni–P2 and C5–Ni–N planes (γ) compared to 76.58° in the X-ray single-crystal structure of **5a**. The Ni–C1 bonds (1.924 Å in **Sa5** and 1.927 Å in **Sa′5**) and Ni–C5 bonds (1.866 Å in both **Sa5** and **Sa′5**) are slightly shorter compared to those in **5a** [1.9340(13) Å and 1.9095(13) Å, respectively]. The C5–N (1.171 Å) bond lengths are considerably longer in **Sa5** and **Sa′5** than **5a** (1.1059(17) Å) (see Tables SI1–SI13 for a more comprehensive list of structural parameters).

Selected interatomic distances (Å), angles (°), and the relative Gibbs free energies for **Sa5**–**Se5** and **S5** with respect to the corresponding **Sa1**–**Se1** and **S1** in THF and toluene (in parenthesis) are summarized in Table 6. The average bond lengths for Ni–C1, Ni–C5, and C5–N are 1.925, 1.867, and 1.171 Å, respectively. The interatomic distance between C1 and C5 is 2.733 Å on average. The phenyl ring is almost perpendicular to the square plane of the complex with an average twist angle of 86.06° between the P–Ni–P plane and the phenyl ring (γ).

Correlation between ΔG° and the Number of F Substituents. The correlation between the relative Gibbs free energies (ΔG°) and the number of *o*-F substituents is shown in Figure 6. The C–CN bond activation products become more stable with respect to the corresponding η^2-nitrile complexes by −6.6 kcal/mol in THF and −6.5 kcal/mol in toluene per *o*-F substituent. This is consistent with the experimentally

Table 6. Selected Interatomic Distances (Å), Angles (°), and Relative Gibbs Free Energies (kcal/mol) for Sa5–Se5 and S5

	Ni–C1	Ni–C5	γ^a	$\Delta G^{\circ b}$
Sa5	1.924	1.866	80.84	−9.6 (−6.6)
Sa′5	1.927	1.866	77.58	−8.9 (−6.0)
Sb5	1.923	1.866	89.44	−5.6 (−1.9)
Sb′5	1.923	1.866	88.13	−5.6 (−1.9)
Sc5	1.927	1.866	89.20	−4.5 (−0.9)
Sd5	1.926	1.870	85.60	−17.0 (−13.4)
Se5	1.922	1.866	88.61	−7.4 (−3.5)
S5	1.925	1.867	89.07	−3.9 (−0.4)

[a]Angle between the P–Ni–P plane and the phenyl ring. [b]Relative Gibbs free energies calculated with respect to corresponding **Sa1**–**Se1** and **S1** in THF and toluene (in parenthesis).

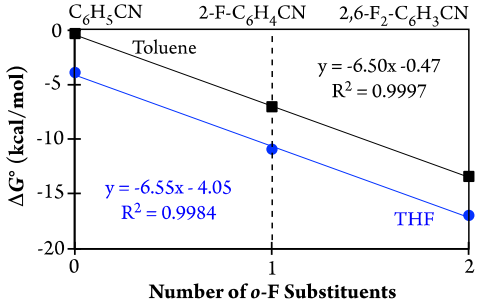

Figure 6. Dependence of calculated ΔG° values on the number of *o*-F substituents.

observed equilibria between these complexes in both THF and toluene.

The correlation between the relative Gibbs free energies (ΔG°) and the number of *m*-F substituents is shown in Figure 7. The C–CN bond activation products become more stable

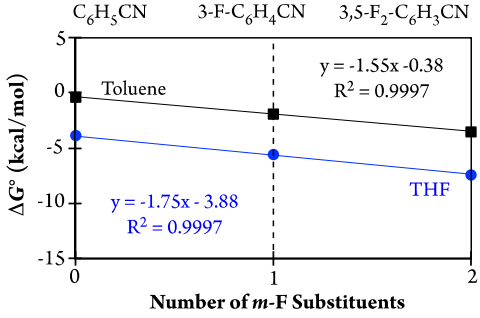

Figure 7. Dependence of calculated ΔG° values on the number of *m*-F substituents.

with respect to the corresponding η^2-nitrile complexes by −1.8 kcal/mol in THF and −1.6 kcal/mol in toluene per *m*-F substituent. This is consistent with the experimentally observed equilibrium between these complexes both in THF and toluene.

Connecting the η^2-Nitrile Complexes to the η^2-Arene Intermediates. TS structures, **TS12**/**TS12′**, connecting the η^2-nitrile complex, **S1**, to the η^2-arene intermediate, **S2**/**S2′**, were located from a relaxed 2D PES scan. Starting from **S1**, in one dimension, the interatomic distance between the nickel metal center and C1 carbon atom was decreased. In the other dimension, the phenyl group was rotated by scanning the P–

https://doi.org/10.1021/acs.organomet.3c00275
Organometallics 2023, 42, 2134–2147

Ni−C1−C2 dihedral angle. **TS12**/**TS12′** were located on the saddle points of the 2D PES. Gas phase-optimized structures of **TSa12′** and **TSa′12** are shown in Figure 8. In **TSa12′**, the

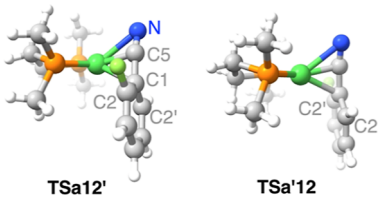

Figure 8. Gas phase-optimized structures of **TSa′12** and **TSa12′**.

fluoro substituent is on the **C2** carbon atom and the nickel metal center is on the **C2′** carbon atom and in **TSa12′**, the fluoro substituent is on the **C2′** carbon atom and the nickel metal center is on the **C2** carbon atom. The initial guess for the TS structures where the nickel metal center and the fluoro substituent are attached to the same carbon atom (**TSa12** and **TSa′12′**) converged to other TS structures. The difference between the relative Gibbs free energies ($\Delta G^{\ddagger}$) of **TSa12′** and **TSa′12** with respect to **Sa′1** is negligible.

The optimized structures of **TSa12′** and **TSa′12** are in good agreement with the previously published TS structure with benzonitrile.[31] The nitrile group is almost linear with the C1−C5−N angle (α) of 171.18° in **TSa12′** and 170.94° in **TSa′12** compared to 139.01° in **Sa′1** and 177.91° in **Sa′2**. The twist angle between the P1−Ni−P2 and C5−Ni−N planes (β) is 62.81° in **TSa12′** and 67.60° in **TSa′12** compared to 1.55° in **Sa′1**, indicating significant deviation from the square planar coordination environment around the nickel metal center. The C5−N bond in **TSa12′**/**TSa′12** (1.184 Å) is much closer to that in **Sa′2** (1.167 Å) compared to **Sa′1** (1.234 Å). The nitrile coordinates to the nickel metal center through the nitrile carbon, and the Ni−C5 bond is 2.016 Å in **TSa12′** and 2.014 Å in **TSa′12**. The Ni−N interatomic distance is significantly elongated in **TSa12′** (2.431 Å) and **TSa′12** (2.431 Å) compared to that in **Sa′1** (1.900 Å). The Ni−C1 bond (2.381 Å in **TSa12′** and 2.382 Å in **TSa′12**) is much shorter than the Ni−C2′ bond in **TSa12′** (2.903 Å) and Ni−C2 bond in **TSa′12** (2.917 Å) compared to their almost equal length in **Sa′2** (1.983 Å and 1.996 Å). The C1−C5 bond length stays relatively constant through this transition (1.428 Å in **TSa12′**/**TSa′12**, 1.461 Å in **Sa′1**, and 1.435 Å in **Sa′2**) (see Tables SI1−SI13 for a more comprehensive list of structural parameters). A comparison of selected interatomic distances (Å) and angles (°) for the optimized structures of **TSa12**−**TSe12** and **TS12** with their relative Gibbs free energies ($\Delta G^{\ddagger}$) with respect to the corresponding structures **Sa1**−**Se1** and **S1** in THF and toluene (in parenthesis) are summarized in Table 7.

The optimized structures of all four possible TS structures with 3-fluorobenzonitrile are shown in Figure SI2 and the optimized structures of **TSc12**−**TSe12** and **TS12** are shown in Figure SI3−SI6. As in **TSa12′** and **TSa′12**, the nitrile group is almost linear with the average C1−C5−N angle (α) of 172.16°. The coordination environment around the nickel metal center significantly deviates from square planar geometry with the average twist angle between the P1−Ni−P2 and C5−Ni−N planes (β) being 64.61°. The average C5−N bond length (1.184 Å) is much closer to that in the η^2-arene complex (**S2**) compared to the η^2-nitrile complex. The nitrile coordinates to the nickel metal center through the nitrile carbon with the average Ni−C5 bond length of 2.019 Å compared to the average Ni−N interatomic distance of 2.398 Å. The average Ni−C1 bond (2.399 Å) is shorter compared to the average Ni−C2/C2′ interatomic distance (2.836 Å), which indicates the formation of the Ni−C1 bond prior to the Ni−C2/C2′ bond. **TSd12**/**TSd12′** have the shortest Ni−C1 bond and **TSe12**/**TSe12′** have the shortest Ni−N and Ni−C2/C2′ interatomic distances. The C1−C5 bond length (1.430 Å on average) stays relatively constant throughout these TS structures and the vibrational mode is a rocking motion of the nickel metal center between the nitrile nitrogen atom and the *ipso* carbon atom of the phenyl ring.

Connecting the C−CN Bond Activation Products to the η^2-Arene Intermediates. TS structures, **TS25**/**TS2′5**, connecting the η^2-arene intermediates, **S2**/**S2′**, to the C−CN bond activation product, **S5**, were located from a second relaxed 2D PES scan. Starting from **S5**, in one dimension, the interatomic distance between C1 and C5 was decreased. In the other dimension, the phenyl group was rotated by scanning the P−Ni−C1−C2 dihedral angle. **TS25**/**TS2′5** were located on the saddle points on the 2D PES. Gas phase-optimized

Table 7. Selected Interatomic Distances (Å), Angles (°), and Relative Gibbs Free Energies for TSa12−TSe12 and TS12

	Ni−C1	Ni−C2/2′	Ni−C5	Ni−N	C1−C5	α^a	β^b	θ^c	$\Delta G^{\ddagger d}$
TSa12′	2.381	2.903	2.016	2.431	1.428	171.18	62.81	71.24	28.2 (26.5)
TSa′12	2.382	2.917	2.014	2.432	1.428	170.94	67.60	76.30	28.0 (26.4)
TSb12	2.416	2.769	2.026	2.384	1.428	173.31	62.43	68.87	28.0 (26.9)
TSb′12	2.399	2.767	2.028	2.402	1.428	173.25	63.52	69.99	28.0 (26.9)
TSb12′	2.403	2.768	2.027	2.404	1.428	173.16	60.35	66.91	28.2 (27.0)
TSb′12′	2.412	2.768	2.026	2.386	1.428	173.13	58.28	64.89	28.1 (26.9)
TSc12	2.447	2.866	2.021	2.424	1.432	173.06	68.33	74.34	27.9 (26.8)
TSc12′	2.448	2.867	2.021	2.424	1.432	172.91	63.96	70.09	28.2 (27.0)
TSd12	2.327	2.971	2.000	2.554	1.434	170.29	76.91	83.12	28.8 (27.7)
TSd12′	2.350	3.014	1.985	2.554	1.437	167.57	75.94	83.65	28.6 (27.7)
TSe12	2.386	2.732	2.026	2.366	1.426	172.12	59.71	66.61	28.2 (27.1)
TSe12′	2.385	2.725	2.026	2.370	1.426	172.20	56.17	63.01	28.3 (27.2)
TS12	2.428	2.816	2.028	2.416	1.431	173.71	66.20	72.20	27.6 (26.4)
TS12′	2.428	2.821	2.027	2.418	1.431	173.47	62.28	68.49	27.8 (26.5)

[a]C1−C5−N angle. [b]Angle between the P1−Ni−P2 and C5−Ni−N planes. [c]Angle between the P1−Ni−P2 and C1−Ni−C5 planes. [d]Relative Gibbs free energies calculated with respect to corresponding **Sa1**−**Se1**, **S1** in THF (numbers in the parenthesis are in toluene).

https://doi.org/10.1021/acs.organomet.3c00275
Organometallics 2023, 42, 2134−2147

structures of **TSa25**, **TSa′25**, **TSa2′5**, and **TSa′2′5** are shown in Figure 9. These TS structures are in good agreement with

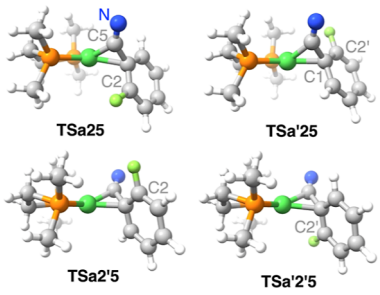

Figure 9. Gas phase-optimized structures of **TSa25**, **TSa′25**, **TSa2′5**, and **TSa′2′5**.

the previously published TS structure with benzonitrile.[31] TS structures where the nickel metal center and the fluoro substituent are attached to the carbon atom (**TSa25**/**TSa′2′5**) are slightly higher in energies than TS structures where the nickel metal center and the fluoro substituent are on opposite sides (**TSa′25**/**TSa2′5**).

In the following discussion, the important geometrical parameters of the lowest energy TS structure, **TSa2′5**, are compared to those in the optimized geometries of the lowest energy η^2-arene intermediate, **Sa2′**, and the C−CN bond activation product, **Sa5**. The nitrile group deviates from linearity with the C1−C5−N angle (α) of 143.81° in **TSa2′5** compared to 178.19° in **Sa2′** and 142.77° in **Sa5**. The twist angle between the P1−Ni−P2 and C1−Ni−C5 planes (θ) is 37.3° in **TSa2′5** compared to 3.39° in **Sa5**, indicating significant deviation from the square planar coordination environment around the nickel metal center. The C5−N bond in **TSa2′5** (1.188 Å) is slightly longer than those in **Sa2′** (1.167 Å) and **Sa5** (1.171 Å). The Ni−C5 bond (1.896 Å in **TSa2′5**) is almost at its final bond length of 1.866 Å in **Sa5**. The Ni−C1 bond (2.028 Å) is slightly longer in **TSa2′5** compared to **Sa2′** (1.978 Å) and **Sa5** (1.924 Å). The C1−C5 bond length is considerably elongated in **TSa2′5** (1.551 Å) compared to **Sa2′** (1.435 Å) (see Table SI1 in the Supporting Information). A comparison of selected interatomic distances (Å) and angles (°) for the optimized structures of **TSa25**−**TSe25** and **TS25** with their relative Gibbs free energies ($\Delta G^{\ddagger}$) with respect to the corresponding **Sa1**−**Se1** and **S1** in THF and toluene (in parenthesis) are summarized in Table 8. The optimized structures of all TS structures are shown in Figures SI1−SI6.

Looking at average metrics for transition-state structures **TSa25**−**TSe25**, the nitrile group is bent with the average C1−C5−N angle (α) of 142.25° as in **TSa2′5**. The coordination environment around the nickel metal center significantly deviates from the square planar geometry with the average twist angle between the P1−Ni−P2 and C1−Ni−C5 planes (θ) at 35.68°. The average C5−N bond length (1.189 Å) is consistent with a triple bond. The average Ni−C5 bond length of 1.887 Å indicates almost complete formation of this bond (1.866 Å). The average C1−C5 bond length (1.564 Å) is considerably elongated compared to 1.435 Å in **Sa2′**. The shortest Ni−C5 bond (1.867 Å) and the longest C1−C5 bond (1.602 Å) are in **TSc2′5**, representing a late TS. On the contrary, the longest Ni−C5 bond (1.928 Å) and the shortest C1−C5 bond (1.499 Å) are in **TSd2′5**, representing the earliest TS. According to Hammond's postulate, the more stable product should have a lower energy TS. This suggests that the activation energy of a step will be inversely proportional to the stability of the product.[68] Unexpectedly though, that is not the case here due to steric hindrance. The Ni−C1 bond length (2.042 Å on average) stays relatively constant through these TS structures and the vibrational mode is a bond stretching between the C1 and C5 carbon atoms (see Tables SI1−SI13 for a more comprehensive list of structural parameters). The relative Gibbs free energies ($\Delta G^{\ddagger}$) with respect to the corresponding **Sa1**−**Se1** and **S1** in THF and toluene (in parenthesis) are very similar with no correlation with the number of the *o*-F or *m*-F substituents.

After connecting the η^2-nitrile complexes, **S1**, and the C−CN bond activation products, **S5**, to the η^2-arene intermediates, **S2**/**S2′** through TS structures, **TS12**/**TS12′** and **TS25**/**TS2′5**, respectively, we then located the TS structures connecting the η^2-arene intermediates, **S2**/**S2′** to **S3**/**S3′** and

Table 8. Selected Interatomic Distances (Å), Angles (°), and Relative Gibbs Free Energies for TSa25−TSe25 and TS25

	Ni−C1	Ni−C2/2′	Ni−C5	C1−C5	C5−N	α^a	β^b	θ^c	$\Delta G^{\ddagger d}$
TSa25	2.095	2.815	1.907	1.520	1.190	144.97	59.77	45.45	27.2 (27.1)
TSa′25	2.012	2.753	1.883	1.567	1.187	142.74	56.59	45.30	25.1 (25.1)
TSa2′5	2.028	2.736	1.896	1.551	1.188	143.81	48.51	37.30	25.0 (25.1)
TSa′2′5	2.100	2.815	1.921	1.513	1.191	145.53	52.34	39.24	28.5 (28.2)
TSb25	2.030	2.699	1.878	1.580	1.189	140.31	44.67	31.07	25.1 (25.9)
TSb′25	2.033	2.707	1.881	1.575	1.189	140.79	45.20	32.29	25.2 (25.9)
TSb2′5	2.028	2.715	1.875	1.586	1.189	140.15	41.28	28.54	25.7 (26.3)
TSb′2′5	2.026	2.707	1.873	1.590	1.189	139.77	41.28	27.60	25.5 (26.1)
TSc25	2.036	2.755	1.874	1.586	1.190	139.97	39.23	27.13	25.2 (26.0)
TSc2′5	2.027	2.760	1.867	1.602	1.190	139.22	36.92	24.31	25.3 (26.1)
TSd25	2.066	2.833	1.908	1.510	1.188	148.19	68.89	60.97	27.2 (27.0)
TSd2′5	2.079	2.842	1.928	1.499	1.188	149.59	63.30	53.53	26.4 (26.4)
TSe25	2.026	2.661	1.884	1.571	1.189	141.09	48.65	34.63	25.3 (25.9)
TSe2′5	2.025	2.669	1.880	1.577	1.189	140.65	44.44	30.85	25.8 (26.3)
TS25	2.035	2.745	1.875	1.588	1.189	139.98	39.83	27.82	25.0 (25.7)
TS2′5	2.027	2.750	1.869	1.602	1.189	139.30	37.12	24.78	25.2 (25.9)

[a]C1−C5−N angle. [b]Angle between the P1−Ni−P2 and C5−Ni−N planes. [c]Angle between the P1−Ni−P2 and C1−Ni−C5 planes. [d]Relative Gibbs free energies calculated with respect to corresponding **Sa1**−**Se1**, **S1** in THF (numbers in the parenthesis are in toluene).

https://doi.org/10.1021/acs.organomet.3c00275
Organometallics 2023, 42, 2134−2147

S4/S4′. Six TS structures, TS22′, TS23/TS2′3′, TS34/TS3′4′, and TS44′ located between six η^2-arene intermediates are discussed in the Supporting Information.

Analysis of the Overall Free Energy Landscape. The energetics of the lowest energy structures along the C−C bond activation of 2-fluorobenzonitrile by the [Ni(dmpe)] fragment is shown in Figure 10. Solvent corrected Gibbs free energies

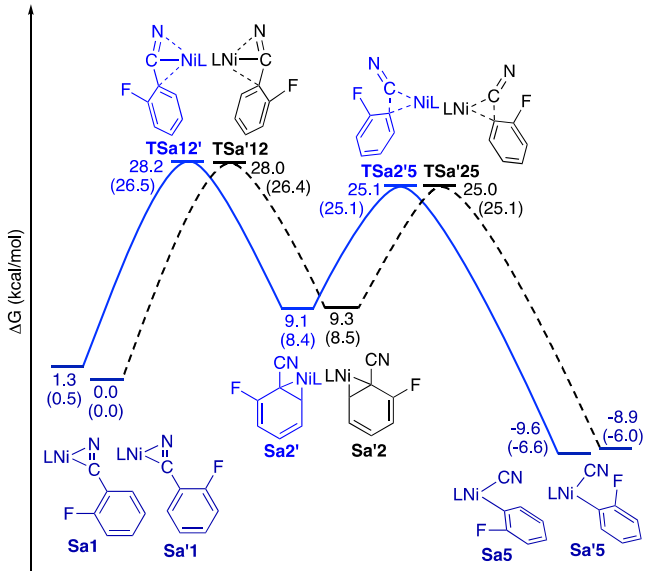

Figure 10. Energetics of C−C bond activation of 2F-benzonitrile by [Ni(dmpe)] fragment relative to the η^2-nitrile complex. SMD-corrected free energies in THF (toluene in parenthesis) are in kcal/mol. Solid blue line: **Sa1** to **Sa5**; dashed black line: **Sa′1** to **Sa′5**.

(kcal/mol) are in THF (toluene in parenthesis) and referenced to the η^2-nitrile complex, **Sa′1**. The C−C bond activation of 2-fluorobenzonitrile by the [Ni(dmpe)] fragment is exothermic by 9.6 kcal/mol in THF and 6.6 kcal/mol in toluene. In the lowest energy pathways, **Sa1** is connected to **Sa5** through **TSa12′**, **Sa2′**, and **TSa2′5** (blue, solid line) and **Sa′1** is connected to **Sa′5** through **TSa′12**, **Sa′2**, and **TSa′25** (black, dashed line). In these structures, the fluoro substituent and the nickel metal center are on the opposite sides of the phenyl ring. Structures where the fluoro substituent and the nickel metal center are attached to the same carbon atom (**Sa2**, **TSa25** and **Sa′2′**, **TSa′2′5**) are higher in energy and are not shown in this figure (see Figure SI7 for all structures). During the optimization of **TSa12** and **TSa′12′**, the phenyl ring rotated due to the steric repulsion between the fluoro substituent and the nickel metal center. The energy difference between these two pathways is negligible. The barrier between **Sa′1** and **Sa′2** is 3.0 kcal/mol higher in energy than the barrier between **Sa′2** and **Sa′5**. The energy of **Sa′2** is 9.3 kcal/mol higher than **Sa′1**.

The energetics of the lowest energy structures along the migration of the [Ni(dmpe)] fragment on the phenyl ring of 2-fluorobenzonitrile to give the η^2-arene complexes is shown in Figure 11. Solvent-corrected Gibbs free energies (kcal/mol) are in THF (toluene in parenthesis) and referenced to the η^2-nitrile complex, **Sa′1**. **Sa2** is connected to **Sa2′** through **TSa22′** (dark blue, solid line) and **Sa′2** is connected to **Sa′2′** through **TSa′22′** (dark blue, dashed line). **Sa2** is connected to **Sa4** through **TSa23**, **Sa3**, and **TSa34** (black, solid line). **Sa′2′** is connected to **Sa′4′** through **TSa′2′3′**, **Sa′3′**, and **TSa′3′4′** (blue, dashed line). **Sa4** is connected to **Sa4′** through **TSa44′** (dark blue, solid line) and **Sa′4** is connected to **Sa′4′** through **TSa′44′** (dark blue, dashed line). The energy difference between these pathways is negligible. Except for **Sa′2** and **Sa2′**, the fluoro substituent and the nickel metal center are on the same side of the phenyl ring in these structures. Structures where the fluoro substituent and the nickel metal center are attached to the opposite sides of the phenyl ring (**TSa2′3′**, **Sa3′**, **TSa3′4′** and **TSa′23**, **Sa′3**, **TSa′34**) are higher in energy and are not shown in this figure (see Figure SI8 for all structures). The barrier between **Sa′2′** and **Sa′3′** is 3.4 kcal/mol lower in energy than the barrier between **Sa′3′** and **Sa′4′**. The highest energy barrier is **TSa′3′4′** with 19.6 kcal/mol. The energy of **Sa′3′** is 1.7 kcal/mol higher than that of **Sa′2** and **Sa′4′**. Relatively low energy transitions between the η^2-arene intermediates are consistent with the experimental data at low temperatures.[31]

The energetics of the lowest energy structures along the C−C bond activation of 3-fluorobenzonitrile by the [Ni(dmpe)] fragment is shown in Figure 12. Solvent-corrected Gibbs free energies (kcal/mol) are in THF (toluene in parenthesis) and referenced to the η^2-nitrile complex, **Sb1**. The C−C bond

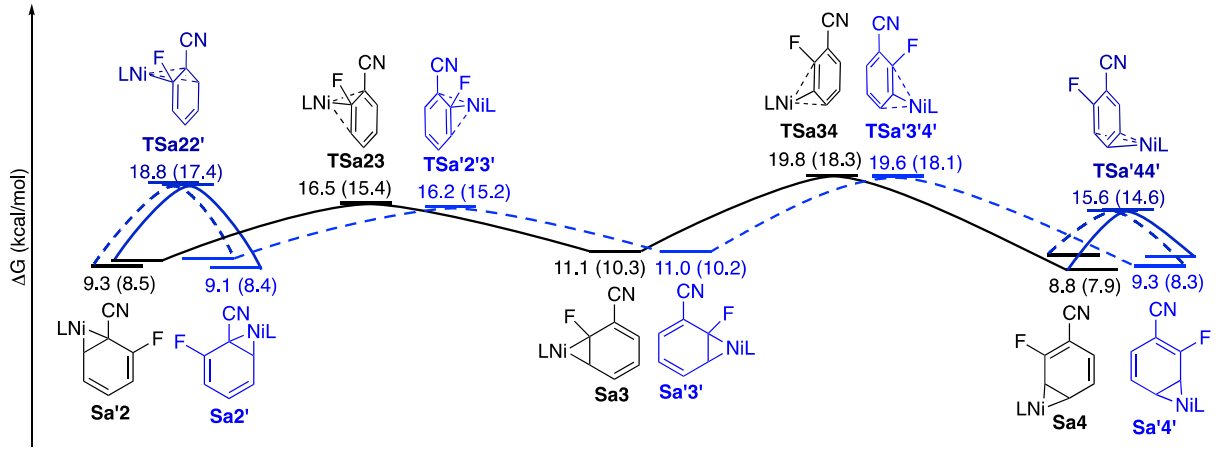

Figure 11. Energetics of η^2-arene complexes of [Ni(dmpe)] relative to the η^2-nitrile complex in the C−C bond activation reaction of 2F-benzonitrile. SMD-corrected free energies in THF (toluene in parenthesis) are in kcal/mol. Solid black line: **Sa2** to **Sa4**; dashed blue line: **Sa′2′** to **Sa′4′**; solid dark blue lines: **Sa2** to **Sa2′**and **Sa4** to **Sa4′**; dashed dark blue lines: **Sa′2** to **Sa′2′** and **Sa′4** to **Sa′4′**.

https://doi.org/10.1021/acs.organomet.3c00275
Organometallics 2023, 42, 2134−2147

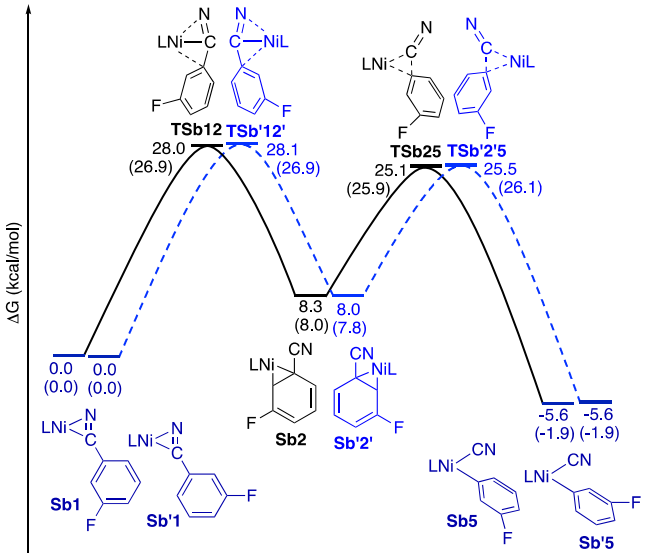

Figure 12. Energetics of C−C bond activation of 3F-benzonitrile by the [Ni(dmpe)] fragment relative to the η^2-nitrile complex. SMD-corrected free energies in THF (toluene in parenthesis) are in kcal/mol. Solid black line: **Sb1** to **Sb5**; dashed blue line: **Sb′1** to **Sb′5**.

activation of 3-fluorobenzonitrile by the [Ni(dmpe)] fragment is exothermic by 5.6 kcal/mol in THF and 1.9 kcal/mol in toluene. **Sb1** is connected to **Sb5** through **TSb12**, **Sb2**, and **TSb25** (black, solid line). **Sb′1** is connected to **Sb′5** through **TSb′12′**, **Sb′2′**, and **TSb′2′5** (blue, dashed line). In these structures, the fluoro substituent and the nickel metal center are on the same side of the phenyl ring. Structures where the fluoro substituent and the nickel metal center are on the opposite sides of the phenyl ring (**TSb12′**, **Sb2′**, **TSb2′5** and **TSb′12**, **Sb′2**, **TSb′25**) are higher in energy and are not shown in this figure (see Figures SI9 for all structures). The energy difference between these pathways is negligible. The barrier between **Sb1** and **Sb2** is 2.9 kcal/mol higher in energy than the barrier between **Sb2** and **Sb5**. The energy of **Sb2** is 8.3 kcal/mol higher than that of **Sb1**. As in 2-fluorobenzonitrile, the transitions between the η^2-arene intermediates have relatively lower energy barriers compared to **TSb12** and **TSb25**. The energetics of migration of the [Ni(dmpe)] fragment on the phenyl ring of 3-fluorobenzonitrile is shown in Figure SI10.

The energetics of the C−C bond activation of 4-fluorobenzonitrile by the [Ni(dmpe)] fragment is shown in Figure 13. Solvent-corrected Gibbs free energies (kcal/mol) are in THF (toluene in parenthesis) and referenced to the η^2-nitrile complex, **Sc1**. The C−C bond activation of 4-fluorobenzonitrile by the [Ni(dmpe)] fragment is exothermic by 4.5 kcal/mol in THF and 0.9 kcal/mol in toluene. **Sc1** is connected to **Sc5** through **TSc12**, **Sc2**, and **TSc25** (black, solid line) and **TSc12′**, **Sc2′**, and **TSc2′5** (blue, solid line). The energy difference between these pathways is negligible. The barrier between **Sc1** and **Sc2** is 2.7 kcal/mol higher in energy than the barrier between **Sc2** and **Sc5**. The energy of **Sc2** is 10.4 kcal/mol higher than **Sc1**. As in 2-fluorobenzonitrile and 3-fluorobenzonitrile, the transitions between the η^2-arene intermediates have relatively lower energy barriers compared to **TSc12** and **TSc25** and the energetics of migration of the [Ni(dmpe)] fragment on the phenyl ring of 4-fluorobenzonitrile is shown in Figure SI12.

The energetics of the C−C bond activation of 2,6-difluorobenzonitrile by the [Ni(dmpe)] fragment is shown in

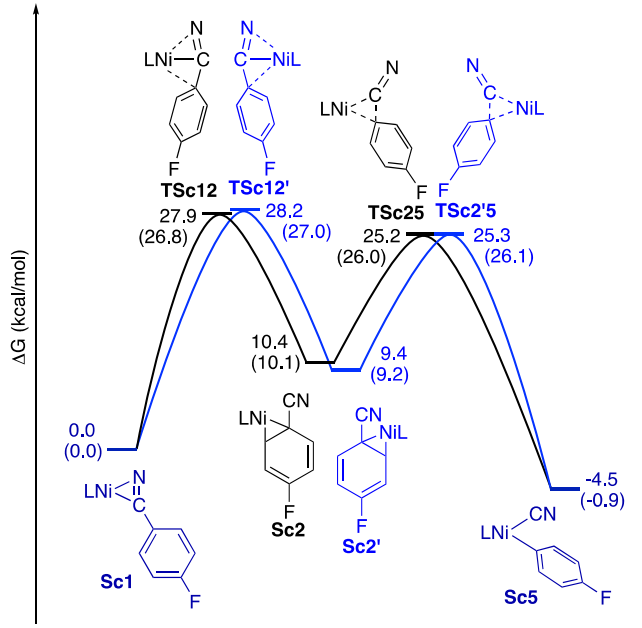

Figure 13. Energetics of C−C bond activation of 4F-benzonitrile by the [Ni(dmpe)] fragment relative to the η^2-nitrile complex. SMD-corrected free energies in THF (toluene in parenthesis) are in kcal/mol. Solid black line: **Sc1** to **Sc5** through **Sc2**; solid blue line: **Sc1** to **Sc5** through **Sc2′**.

Figure 14. Solvent-corrected Gibbs free energies (kcal/mol) are in THF (toluene in parenthesis) and referenced to the η^2-nitrile complex, **Sd1**. The C−C bond activation of 2,6-difluorobenzonitrile by the [Ni(dmpe)] fragment is exothermic by 17.0 kcal/mol in THF and 13.4 kcal/mol in toluene. **Sd1** is connected to **Sd5** through **TSd12**, **Sd2**, and **TSd25** (black, solid line) and **TSd12′**, **Sd2′**, and **TSd2′5** (blue, solid

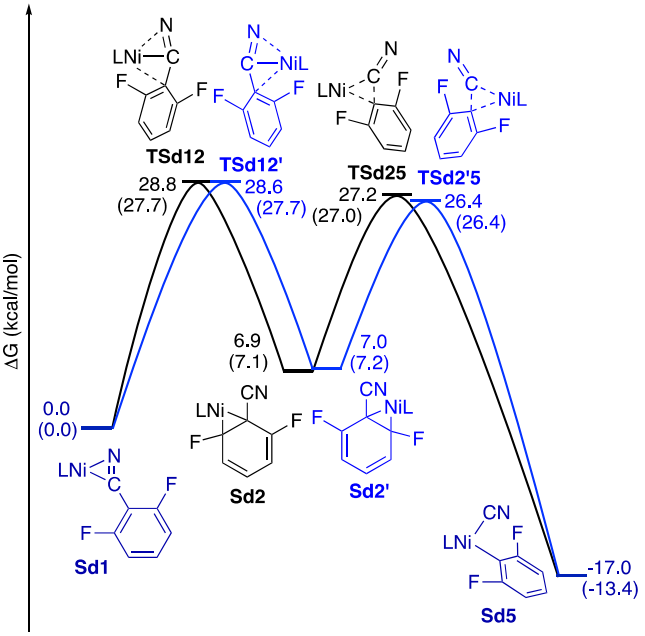

Figure 14. Energetics of C−C bond activation of 2,6-F_2-benzonitrile by the [Ni(dmpe)] fragment relative to the η^2-nitrile complex. SMD-corrected free energies in THF (toluene in parenthesis) are in kcal/mol. Solid black line: **Sd1** to **Sd5** through **Sd2**; solid blue line: **Sd1** to **Sd5** through **Sd2′**.

https://doi.org/10.1021/acs.organomet.3c00275
Organometallics 2023, 42, 2134−2147

line). The energy difference between these pathways is negligible. The barrier between **Sd1** and **Sd2′** is 2.2 kcal/mol higher in energy than the barrier between **Sd2′** and **Sd5**. The energy of **Sd2′** is 7.0 kcal/mol higher than that of **Sd1**. Transitions between the η^2-arene intermediates have relatively lower energy barriers compared to **TSd12** and **TSd25** and the energetics of migration of the [Ni(dmpe)] fragment on the phenyl ring of 2,6-difluorobenzonitrile is shown in Figure SI14. Also, the η^2-arene complex, **Sd2**, is lower in energy relative to the η^2-nitrile complex, **Sd1**, than in any of the other fluorobenzonitriles.

The energetics of the C−C bond activation of 3,5-difluorobenzonitrile by the [Ni(dmpe)] fragment is shown in Figure 15. Solvent-corrected Gibbs free energies (kcal/mol)

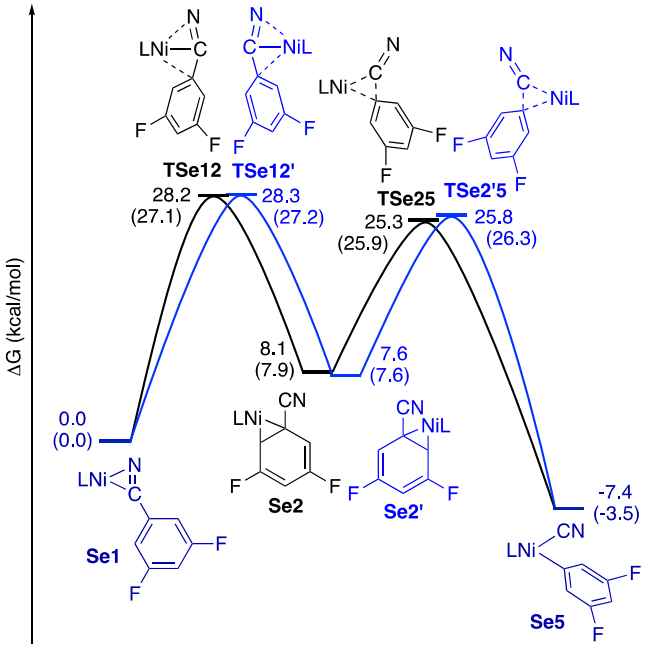

Figure 15. Energetics of C−C bond activation of 3,5-F_2-benzonitrile by the [Ni(dmpe)] fragment relative to the η^2-nitrile complex. SMD-corrected free energies in THF (toluene in parenthesis) are in kcal/mol. Solid black line: **Se1** to **Se5** through **Se2**; solid blue line: **Se1** to **Se5** through **Se2′**.

are in THF (toluene in parenthesis) and referenced to the η^2-nitrile complex, **Se1**. The C−C bond activation of 3,5-difluorobenzonitrile by the [Ni(dmpe)] fragment is exothermic by 7.4 kcal/mol in THF and 3.5 kcal/mol in toluene. **Se1** is connected to **Se5** through **TSe12**, **Se2**, and **TSe25** (black, solid line) and **TSe12′**, **Se2′**, and **TSe2′5** (blue, solid line). The energy difference between these pathways is negligible. The barrier between **Se1** and **Se2** is 2.9 kcal/mol higher in energy than the barrier between **Se2** and **Se5**. The energy of **Se2** is 8.1 kcal/mol higher than that of **Se1**. Transitions between the η^2-arene intermediates have relatively lower energy barriers compared to **TSe12** and **TSe25**, and the energetics of migration of the [Ni(dmpe)] fragment on the phenyl ring of 3,5-difluorobenzonitrile is shown in Figure SI16.

The frontier molecular orbitals for the C−C bond activation product of 2,6-difluorobenzonitrile calculated by the natural bond orbital analysis is shown in Figure 16. The highest energy occupied molecular orbital (HOMO) is the d_{z^2} orbital of the nickel metal center. The lowest energy unoccupied molecular

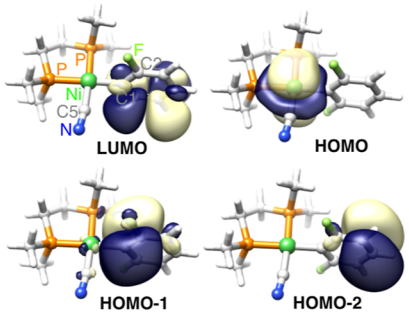

Figure 16. Frontier molecular orbitals for the C−C bond activation product of 2,6-F_2-C_6H_4.

orbital (LUMO), second highest energy occupied molecular orbital (HOMO-1), and third highest energy occupied molecular orbital (HOMO-2) are located on the phenyl ring. HOMO-1 and HOMO-2 are π bonding and LUMO is a π^* antibonding orbital.

The energies of the frontier molecular orbitals for the C−C bond activation product of benzonitrile, 2-fluorobenzonitrile, and 2,6-difluorobenzonitrile are shown in Table 9. The

Table 9. Energies (eV) of the Frontier Molecular Orbitals for the C−C Bond Activation Products of Benzonitrile, and 2-Fluoro- and 2,6-Difluorobenzonitrile

	C_6H_5CN	2-F-C_6H_4CN	2,6-F_2-C_6H_3CN
LUMO	0.04743	0.03591	0.03047
HOMO	−0.21368	−0.21643	−0.21998
HOMO-1	−0.21704	−0.22355	−0.24645
HOMO-2	−0.22940	−0.23779	−0.24684

energies of the 2,6-difluorobenzonitrile frontier molecular orbitals are the lowest, followed by those of 2-fluorobenzonitrile and benzonitrile. The HOMO-1 and HOMO-2 energies are almost the same in the C−C bond activation product of 2,6-difluorobenzonitrile. This indicates that the fluoro substituents stabilize HOMO-1 more than HOMO-2. The HOMO-2 is at a lower energy than HOMO-1 in the C−C bond activation product of benzonitrile and 2-fluorobenzonitrile.

CONCLUSIONS

The effect of fluoro substitution on the C−C bond activation of benzonitrile has been studied by reacting five fluoro-substituted benzonitriles with the [Ni(dippe)] fragment. Relative Gibbs free energies (ΔG°) were obtained from the Van't Hoff plots for the C−C bond activation of 3-fluoro- and 4-fluorobenzonitrile. X-ray single-crystal structures for the η^2-nitrile complexes and the C−CN bond activation products were used as the starting geometries for the DFT calculations, and reaction intermediates and TS structures on the PES were located with the [Ni(dmpe)] fragment. The C−CN bond activation products were found to be more stable with respect to the corresponding η^2-nitrile complexes by −6.6 kcal/mol in THF and −6.5 kcal/mol in toluene per *o*-F substituent and by −1.8 kcal/mol in THF and −1.6 kcal/mol in toluene per *m*-F substituent. This is consistent with the inductive effect of the *ortho* fluorine observed for the C−H bond activation.[69] Similar to the C−C bond activation of benzonitrile,[31] the C−C bond being activated is not in the square plane of the nickel metal center in the C−C bond activation TS, and a higher energy η^2-

https://doi.org/10.1021/acs.organomet.3c00275
Organometallics 2023, 42, 2134−2147

arene intermediate is formed prior to C−C bond activation. This mechanistic study can lead to further progress in the development of synthetic methods for the construction of fluorinated compounds.

■ ASSOCIATED CONTENT

Supporting Information

The Supporting Information is available free of charge at https://pubs.acs.org/doi/10.1021/acs.organomet.3c00275.

^{1}H, ^{13}C, ^{31}P{^{1}H}, and ^{19}F NMR spectra, full details of the X-ray structure determinations, experimental and computational details, thermodynamic parameters calculated from the van't Hoff plot, energies, optimized geometries, and Cartesian coordinates of optimized structures (PDF)

xyz coordinate files (XYZ)

Accession Codes

CCDC 2255206−2255215 contain the supplementary crystallographic data for this paper. These data can be obtained free of charge via www.ccdc.cam.ac.uk/data_request/cif, or by emailing data_request@ccdc.cam.ac.uk, or by contacting The Cambridge Crystallographic Data Centre, 12 Union Road, Cambridge CB2 1EZ, UK; fax: +44 1223 336033.

■ AUTHOR INFORMATION

Corresponding Authors

Abdurrahman C. Atesin − *Department of Chemistry, The University of Texas Rio Grande Valley, Edinburg, Texas 78541, United States*; Email: abdurrahman.atesin@utrgv.edu

Tülay A. Ateşin − *Department of Chemistry, The University of Texas Rio Grande Valley, Edinburg, Texas 78541, United States*; orcid.org/0000-0001-8394-8830; Email: tulay.atesin@utrgv.edu

William D. Jones − *Department of Chemistry, University of Rochester, Rochester, New York 14627, United States*; orcid.org/0000-0003-1932-0963; Email: jones@chem.rochester.edu

Authors

Sébastien Lachaize − *Department of Chemistry, University of Rochester, Rochester, New York 14627, United States*

Dominique C. Gallegos − *Department of Chemistry, The University of Texas Rio Grande Valley, Edinburg, Texas 78541, United States*

Juliana J. Antonio − *Department of Chemistry, The University of Texas Rio Grande Valley, Edinburg, Texas 78541, United States*

Complete contact information is available at: https://pubs.acs.org/10.1021/acs.organomet.3c00275

Author Contributions

§S.L. and D.C.G. contributed equally. The manuscript was written through contributions of all authors.

Funding

We acknowledge support from the U.S. Department of Energy, Basic Energy Sciences (BES) Chemical Sciences, Geosciences, & Biosciences (CSGB) Division (DE-SC0020230) (W.D.J.) and Robert A. Welch Foundation Departmental Grant (grant no. BX-0048) at the Department of Chemistry at The University of Texas Rio Grande Valley (A.C.A and T.A.A.).

Notes

The authors declare no competing financial interest.

■ ACKNOWLEDGMENTS

W.D.J. acknowledges assistance in obtaining X-ray structures by Drs. Christine J. Flaschenriem and William W. Brennessel at the X-ray Crystallographic Facility of the Department of Chemistry at the University of Rochester. T.A.A. and A.C.A. acknowledge the Texas Advanced Computing Center (TACC) at The University of Texas at Austin for providing HPC resources that have contributed to the research results reported within this paper (URL: http://www.tacc.utexas.edu).

■ ABBREVIATIONS

C−C	carbon−carbon sigma bond
C−CN	carbon−nitrile bond
DFT	density functional theory
dippe	1,2-bis(diisopropylphosphino)ethane
dmpe	1,2-bis(dimethylphosphino)ethane
NMR	nuclear magnetic resonance
PES	potential energy surface
SMD	solvation model based on density
THF	tetrahydrofuran
Tol	toluene
TS	transition structure
ZPE	zero-point energy

■ REFERENCES

(1) Murakami, M.; Ishida, N. Potential of Metal-Catalyzed C−C Single Bond Cleavage for Organic Synthesis. *J. Am. Chem. Soc.* **2016**, *138*, 13759−13769.

(2) Bi, X.; Zhang, Q.; Gu, Z. Transition-Metal-Catalyzed Carbon-Carbon Bond Activation in Asymmetric Synthesis. *Chin. J. Chem.* **2021**, *39*, 1397−1412.

(3) Higashida, K.; Smaïl, V.; Nagae, H.; Carpentier, J.-F.; Mashima, K. Nickel-Catalyzed Asymmetric Allylic Alkylation of *β*-Dicarbonyl Compounds via C−C Bond Activation of 2-Allylated Cyclic 1,3-Diketones. *ACS Catal.* **2023**, *13*, 2156−2161.

(4) Dong, G., Ed.; Springer: Berlin, Heidelberg, 2014; Vol. *346*, pp 1−257.*C-C Bond Activation*Topics in Current Chemistry

(5) Xia, Y.; Lu, G.; Liu, P.; Dong, G. Catalytic Activation of Carbon−Carbon Bonds in Cyclopentanones. *Nature* **2016**, *539*, 546−550.

(6) Lu, G.; Fang, C.; Xu, T.; Dong, G.; Liu, P. Computational Study of Rh-Catalyzed Carboacylation of Olefins: Ligand-Promoted Rhodacycle Isomerization Enables Regioselective C−C Bond Functionalization of Benzocyclobutenones. *J. Am. Chem. Soc.* **2015**, *137*, 8274−8283.

(7) Adams, D. M.; Chatt, J.; Guy, R. G.; Sheppard, N. 149. The Structure of "Cyclopropane Platinous Chloride". *J. Chem. Soc.* **1961**, *0*, 738−742.

(8) Benfield, F. W. S.; Green, M. L. H. Alkyl, Alkynyl, and Olefin Complexes of Bis(*π*-Cyclopentadienyl)-Molybdenum or -Tungsten : A Reversible Metal-to-Ring Transfer of an Ethyl Group. *J. Chem. Soc., Dalton Trans.* **1974**, *12*, 1324−1331.

(9) Suggs, J. W.; Jun, C. H. Directed Cleavage of Carbon−Carbon Bonds by Transition Metals: The *α*-Bonds of Ketones. *J. Am. Chem. Soc.* **1984**, *106*, 3054−3056.

(10) Gozin, M.; Weisman, A.; Ben-David, Y.; Milstein, D. Activation of a Carbon−Carbon Bond in Solution by Transition-Metal Insertion. *Nature* **1993**, *364*, 699−701.

(11) Song, F.; Gou, T.; Wang, B.-Q.; Shi, Z.-J. Catalytic Activations of Unstrained C−C Bond Involving Organometallic Intermediates. *Chem. Soc. Rev.* **2018**, *47*, 7078−7115.

(12) Chen, F.; Wang, T.; Jiao, N. Recent Advances in Transition-Metal-Catalyzed Functionalization of Unstrained Carbon−Carbon Bonds. *Chem. Rev.* **2014**, *114*, 8613−8661.
(13) Murakami, M., Ed.; John Wiley & Sons, Ltd, 2015, pp 1−272.*Cleavage of Carbon-Carbon Single Bonds by Transition Metals*
(14) Song, F.; Gou, T.; Wang, B.-Q.; Shi, Z.-J. Catalytic Activations of Unstrained C−C Bond Involving Organometallic Intermediates. *Chem. Soc. Rev.* **2018**, *47*, 7078−7115.
(15) Nairoukh, Z.; Cormier, M.; Marek, I. Merging C−H and C−C Bond Cleavage in Organic Synthesis. *Nat. Rev. Chem.* **2017**, *1*, 0035−117.
(16) Lutz, M. D. R.; Morandi, B. Metal-Catalyzed Carbon−Carbon Bond Cleavage of Unstrained Alcohols. *Chem. Rev.* **2021**, *121*, 300−326.
(17) Fumagalli, G.; Stanton, S.; Bower, J. F. Recent Methodologies That Exploit C−C Single-Bond Cleavage of Strained Ring Systems by Transition Metal Complexes. *Chem. Rev.* **2017**, *117*, 9404−9432.
(18) Chen, P.; Billett, B. A.; Tsukamoto, T.; Dong, G. "Cut and Sew" Transformations via Transition-Metal-Catalyzed Carbon−Carbon Bond Activation. *ACS Catal.* **2017**, *7*, 1340−1360.
(19) Cohen, Y.; Cohen, A.; Marek, I. Creating Stereocenters within Acyclic Systems by C−C Bond Cleavage of Cyclopropanes. *Chem. Rev.* **2021**, *121*, 140−161.
(20) Vicente, R. C−C Bond Cleavages of Cyclopropenes: Operating for Selective Ring-Opening Reactions. *Chem. Rev.* **2021**, *121*, 162−226.
(21) Souillart, L.; Cramer, N. Catalytic C-C Bond Activations via Oxidative Addition to Transition Metals. *Chem. Rev.* **2015**, *115*, 9410−9464.
(22) Ruhland, K. Transition-Metal-Mediated Cleavage and Activation of C-C Single Bonds. *Eur. J. Org. Chem.* **2012**, *2012*, 2683−2706.
(23) Favero, G.; Morvillo, A.; Turco, A. Oxidative Addition of Alkanenitriles to Nickel(0) Complexes via π-Intermediates. *J. Organomet. Chem.* **1983**, *241*, 251−257.
(24) García, J. J.; Arévalo, A.; Brunkan, N. M.; Jones, W. D. Cleavage of Carbon−Carbon Bonds in Alkyl Cyanides Using Nickel(0). *Organometallics* **2004**, *23*, 3997−4002.
(25) Ateşin, T. A.; Li, T.; Lachaize, S.; Brennessel, W. W.; García, J. J.; Jones, W. D. Experimental and Theoretical Examination of C−CN and C−H Bond Activations of Acetonitrile Using Zerovalent Nickel. *J. Am. Chem. Soc.* **2007**, *129*, 7562−7569.
(26) Ahmad, M. S.; Pulidindi, I. N.; Li, C. Recent Advances in C−CN and C−H Bond Activation of Green Nitrile (MeCN) for Organo-Complexation, Cyanation and Cyanomethylation. *New J. Chem.* **2020**, *44*, 17177−17197.
(27) Abla, M.; Yamamoto, T. Oxidative Addition of C-CN Bond to Nickel(0) Complex: Synthesis and Crystal Structures of Ni(CN)(o-C_6H_4CN) (Bpy) and Ni(CN) (p-C_6H_4CN) (Bpy). *J. Organomet. Chem.* **1997**, *532*, 267−270.
(28) Parshall, G. W. σ-Aryl Compounds of Nickel, Palladium, And Platinum. Synthesis and Bonding Studies. *J. Am. Chem. Soc.* **1974**, *96*, 2360−2366.
(29) Garcia, J. J.; Jones, W. D. Reversible Cleavage of Carbon−Carbon Bonds in Benzonitrile Using Nickel(0). *Organometallics* **2000**, *19*, 5544−5545.
(30) Garcia, J. J.; Brunkan, N. M.; Jones, W. D. Cleavage of Carbon−Carbon Bonds in Aromatic Nitriles Using Nickel(0). *J. Am. Chem. Soc.* **2002**, *124*, 9547−9555.
(31) Ateşin, T. A.; Li, T.; Lachaize, S.; García, J. J.; Jones, W. D. Experimental and Theoretical Examination of C−CN Bond Activation of Benzonitrile Using Zerovalent Nickel. *Organometallics* **2008**, *27*, 3811−3817.
(32) Li, T.; García, J. J.; Brennessel, W. W.; Jones, W. D. C−CN Bond Activation of Aromatic Nitriles and Fluxionality of the η^2-Arene Intermediates: Experimental and Theoretical Investigations. *Organometallics* **2010**, *29*, 2430−2445.
(33) Jones, W.; Swartz, B.; Brennessel, W. Lewis Acid Assisted C−CN Cleavage of Benzonitrile Using $[(dippe)NiH]_2$. *Synlett* **2018**, *29*, 747−753.
(34) Muetterties, E. L.; Gerlach, D. H.; Kane, A. R.; Parshall, G. W.; Jesson, J. P. Reactivity of Trialkylphosphine Complexes of Platinum(0). *J. Am. Chem. Soc.* **1971**, *93*, 3543−3544.
(35) Miller, J. A. C—C Bond Activation with Selective Functionalization: Preparation of Unsymmetrical Biaryls from Benzonitriles. *Tetrahedron Lett.* **2001**, *42*, 6991−6993.
(36) Boehm, P.; Müller, P.; Finkelstein, P.; Rivero-Crespo, M. A.; Ebert, M.-O.; Trapp, N.; Morandi, B. Mechanistic Investigation of the Nickel-Catalyzed Metathesis between Aryl Thioethers and Aryl Nitriles. *J. Am. Chem. Soc.* **2022**, *144*, 13096−13108.
(37) Reilly, S. W.; Lam, Y.; Ren, S.; Strotman, N. A. Late-Stage Carbon Isotope Exchange of Aryl Nitriles through Ni-Catalyzed C−CN Bond Activation. *J. Am. Chem. Soc.* **2021**, *143*, 4817−4823.
(38) Ren, H.; Du, G.-F.; Zhu, B.; Yang, G.-C.; Yao, L.-S.; Guan, W.; Su, Z.-M. Theoretical Mechanistic Study of Nickel(0)/Lewis Acid Catalyzed Polyfluoroarylcyanation of Alkynes: Origin of Selectivity for C−CN Bond Activation. *Organometallics* **2018**, *37*, 2594−2601.
(39) Ohnishi, Y.; Nakao, Y.; Sato, H.; Nakao, Y.; Hiyama, T.; Sakaki, S. A Theoretical Study of Nickel(0)-Catalyzed Phenylcyanation of Alkynes. Reaction Mechanism and Regioselectivity. *Organometallics* **2009**, *28*, 2583−2594.
(40) Acosta-Ramírez, A.; Muñoz-Hernández, M.; Jones, W. D.; García, J. J. Isomerization of 2-Methyl-3-Butenenitrile with (Bis-Diphenylphosphinoferrocene)Nickel Compounds: Catalytic and Structural Studies. *J. Organomet. Chem.* **2006**, *691*, 3895−3901.
(41) Acosta-Ramírez, A.; Flores-Gaspar, A.; Muñoz-Hernández, M.; Arévalo, A.; Jones, W. D.; García, J. J. Nickel Complexes Involved in the Isomerization of 2-Methyl-3-Butenenitrile. *Organometallics* **2007**, *26*, 1712−1720.
(42) Acosta-Ramírez, A.; Muñoz-Hernández, M.; Jones, W. D.; García, J. J. Catalytic Isomerization of 2-Methyl-3-Butenenitrile by Nickel Systems Using Bis-Diphosphinoferrocene Ligands: Evidence for Hemilability. *Organometallics* **2007**, *26*, 5766−5769.
(43) Acosta-Ramírez, A.; Flores-Álamo, M.; Jones, W. D.; García, J. J. P−C Bond Scission at the TRIPHOS Ligand and C−CN Bond Cleavage in 2-Methyl-3-Butenenitrile with $[Ni(COD)_2]$. *Organometallics* **2008**, *27*, 1834−1840.
(44) Acosta-Ramírez, A.; Morales-Morales, D.; Serrano-Becerra, J. M.; Arévalo, A.; Jones, W. D.; García, J. J. Study of the Reactivity of 2-Methyl-3-Butenenitrile with Ni(0)-N-Heterocyclic Carbene Complexes. *J. Mol. Catal. A: Chem.* **2008**, *288*, 14−18.
(45) Swartz, B. D.; Reinartz, N. M.; Brennessel, W. W.; García, J. J.; Jones, W. D. Solvent Effects and Activation Parameters in the Competitive Cleavage of C−CN and C−H Bonds in 2-Methyl-3-Butenenitrile Using $[(Dippe)NiH]_2$. *J. Am. Chem. Soc.* **2008**, *130*, 8548−8554.
(46) Li, T.; Jones, W. D. DFT Calculations of the Isomerization of 2-Methyl-3-Butenenitrile by [Ni(Bisphosphine)] in Relation to the DuPont Adiponitrile Process. *Organometallics* **2011**, *30*, 547−555.
(47) Brunkan, N. M.; Jones, W. D. Preparation, Structure, and Dynamics of a Nickel π-Allyl Cyanide Complex. *J. Organomet. Chem.* **2003**, *683*, 77−82.
(48) Brunkan, N. M.; Brestensky, D. M.; Jones, W. D. Kinetics, Thermodynamics, and Effect of BPh_3 on Competitive C−C and C−H Bond Activation Reactions in the Interconversion of Allyl Cyanide by [Ni(Dippe)]. *J. Am. Chem. Soc.* **2004**, *126*, 3627−3641.
(49) Göthlich, A. P. V.; Tensfeldt, M.; Rothfuss, H.; Tauchert, M. E.; Haap, D.; Rominger, F.; Hofmann, P. Novel Chelating Phosphonite Ligands: Syntheses, Structures, and Nickel-Catalyzed Hydrocyanation of Olefins. *Organometallics* **2008**, *27*, 2189−2200.
(50) Bini, L.; Müller, C.; Wilting, J.; von Chrzanowski, L.; Spek, A. L.; Vogt, D. Highly Selective Hydrocyanation of Butadiene toward 3-Pentenenitrile. *J. Am. Chem. Soc.* **2007**, *129*, 12622−12623.
(51) Chaumonnot, A.; Lamy, F.; Sabo-Etienne, S.; Donnadieu, B.; Chaudret, B.; Barthelat, J.-C.; Galland, J.-C. Catalytic Isomerization of Cyanoolefins Involved in the Adiponitrile Process. C−CN Bond

https://doi.org/10.1021/acs.organomet.3c00275
Organometallics 2023, 42, 2134−2147

Cleavage and Structure of the Nickel π-Allyl Cyanide Complex Ni(η^3-1-Me-C_3H_4)(CN)(dppb). *Organometallics* **2004**, *23*, 3363−3365.
(52) Wilting, J.; Müller, C.; Hewat, A. C.; Ellis, D. D.; Tooke, D. M.; Spek, A. L.; Vogt, D. Nickel-Catalyzed Isomerization of 2-Methyl-3-Butenenitrile. *Organometallics* **2005**, *24*, 13−15.
(53) van der Vlugt, J.; Hewat, A. C.; Neto, S.; Sablong, R.; Mills, A. M.; Lutz, M.; Spek, A. L.; Müller, C.; Vogt, D. Sterically Demanding Diphosphonite Ligands −Synthesis and Application in Nickel-Catalyzed Isomerization of 2-Methyl-3-Butenenitrile. *Adv. Synth. Catal.* **2004**, *346*, 993−1003.
(54) Morvillo, A.; Turco, A. Reactions of Organic Halides and Cyanides with Bis(tricyclohexylphosphine)Nickel(0). *J. Organomet. Chem.* **1981**, *208*, 103−113.
(55) Liu, N.; Wang, Z.-X. Nickel-Catalyzed Cross-Coupling of Arene- or Heteroarenecarbonitriles with Aryl- or Heteroarylmanganese Reagents through C-CN Bond Activation. *Adv. Synth. Catal.* **2012**, *354*, 1641−1645.
(56) Arévalo, A.; García, J. J. Bond Activation with Low-Valent Nickel in Homogeneous Systems. *Eur. J. Inorg. Chem.* **2010**, *2010*, 4063−4074.
(57) Bianchini, C.; Masi, D.; Meli, A.; Sabat, M. Reactions of Ethyl Cyanoformate with (Np_3)Ni, (Np_3)CoH [Np_3 = $N(CH_2CH_2PPh_2)_3$], and (Triphos)Ni [Triphos = $MeC(CH_2PPh_2)_3$]. Crystal Structures of the Ethoxycarbonyl Complexes [(Np_3)Ni(CO_2Et)]BPh_4 and (Triphos)Ni(CN)(CO_2Et). *Organometallics* **1986**, *5*, 1670−1675.
(58) Schaub, T.; Döring, C.; Radius, U. Efficient Nickel Mediated Carbon−Carbon Bond Cleavage of Organonitriles. *Dalton Trans.* **2007**, 1993−2002.
(59) Evans, M. E.; Li, T.; Jones, W. D. C−H vs C−C Bond Activation of Acetonitrile and Benzonitrile via Oxidative Addition: Rhodium vs Nickel and Cp* vs Tp′ (Tp′ = Hydrotris(3,5-Dimethylpyrazol-1-yl)Borate, Cp* = η^5-Pentamethylcyclopentadienyl). *J. Am. Chem. Soc.* **2010**, *132*, 16278−16284.
(60) Grochowski, M. R.; Li, T.; Brennessel, W. W.; Jones, W. D. Competitive Carbon−Sulfur vs Carbon−Carbon Bond Activation of 2-Cyanothiophene with [Ni(dippe)H]$_2$. *J. Am. Chem. Soc.* **2010**, *132*, 12412−12421.
(61) García-Ventura, I.; Flores-Alamo, M.; García, J. Carbon−Carbon vs. Carbon−Oxygen Bond Activation in 2- and 3-Furonitriles with Nickel. *RSC Adv.* **2016**, *6*, 101259−101266.
(62) Watson, M. P.; Jacobsen, E. N. Asymmetric Intramolecular Arylcyanation of Unactivated Olefins via C−CN Bond Activation. *J. Am. Chem. Soc.* **2008**, *130*, 12594−12595.
(63) Nakao, Y.; Ebata, S.; Yada, A.; Hiyama, T.; Ikawa, M.; Ogoshi, S. Intramolecular Arylcyanation of Alkenes Catalyzed by Nickel/$AlMe_2Cl$. *J. Am. Chem. Soc.* **2008**, *130*, 12874−12875.
(64) Fleming, F. F.; Fleming, F. F. Nitrile-Containing Natural Products. *Nat. Prod. Rep.* **1999**, *16*, 597−606.
(65) Fleming, F. F.; Yao, L.; Ravikumar, P. C.; Funk, L.; Shook, B. C. Nitrile-Containing Pharmaceuticals: Efficacious Roles of the Nitrile Pharmacophore. *J. Med. Chem.* **2010**, *53*, 7902−7917.
(66) Delcaillau, T.; Morandi, B. Nickel-Catalyzed Thiolation of Aryl Nitriles. *Chem.—Eur. J.* **2021**, *27*, 11823−11826.
(67) Inoue, M.; Sumii, Y.; Shibata, N. Contribution of Organofluorine Compounds to Pharmaceuticals. *ACS Omega* **2020**, *5*, 10633−10640.
(68) Hammond, G. S. A. A Correlation of Reaction Rates. *J. Am. Chem. Soc.* **1955**, *77*, 334−338.
(69) Evans, M. E.; Burke, C. L.; Yaibuathes, S.; Clot, E.; Eisenstein, O.; Jones, W. D. Energetics of C−H Bond Activation of Fluorinated Aromatic Hydrocarbons Using a [Tp′Rh(CNneopentyl)] Complex. *J. Am. Chem. Soc.* **2009**, *131*, 13464−13473.

https://doi.org/10.1021/acs.organomet.3c00275
Organometallics 2023, 42, 2134−2147